UNIVERSITY OF LEEDS

This is a repository copy of *Visualizing the Stoichiometry of Industrial-Style Co-Mo-S Catalysts with Single-Atom Sensitivity*.

White Rose Research Online URL for this paper:
http://eprints.whiterose.ac.uk/166342/

Version: Accepted Version

Article:
Zhu, Y, Ramasse, QM orcid.org/0000-0001-7466-2283, Brorson, M et al. (4 more authors) (2014) Visualizing the Stoichiometry of Industrial-Style Co-Mo-S Catalysts with Single-Atom Sensitivity. Angewandte Chemie International Edition, 53 (40). pp. 10723-10727. ISSN 1433-7851

https://doi.org/10.1002/anie.201405690

Reuse
Items deposited in White Rose Research Online are protected by copyright, with all rights reserved unless indicated otherwise. They may be downloaded and/or printed for private study, or other acts as permitted by national copyright laws. The publisher or other rights holders may allow further reproduction and re-use of the full text version. This is indicated by the licence information on the White Rose Research Online record for the item.

Takedown
If you consider content in White Rose Research Online to be in breach of UK law, please notify us by emailing eprints@whiterose.ac.uk including the URL of the record and the reason for the withdrawal request.

White Rose university consortium
Universities of Leeds, Sheffield & York

eprints@whiterose.ac.uk
https://eprints.whiterose.ac.uk/

Visualizing the stoichiometry of industrial-style Co-Mo-S catalysts with single-atom sensitivity

Yuanyuan Zhu, Quentin M. Ramasse, Michael Brorson, Poul G. Moses, Lars P. Hansen, Christian F. Kisielowski and Stig Helveg

Transition metal dichalcogenide (TMD) materials have unique physicochemical properties.[1,2] Such functionalities may benefit from incorporating other elements into the TMD structure.[3,4] For instance, chemical promotion is significant for nanocrystalline MoS_2 applied in catalytic hydrotreating desulfurization (HDS) processing of crude oil fractions. Here, promotion by transition metals such as Co (or Ni) is attributed to the so-called "Co-Mo-S" phase.[3] The Co-Mo-S phase was identified as consisting of Co atoms attached to the catalytically important edges of the MoS_2 nanocrystals using spectroscopic techniques.[3] An atomic structure for the Co-Mo-S phase was proposed based on complementary model studies using scanning tunneling microscopy (STM)[5,6] and density functional theory (DFT) calculations.[6,7] However, relating the model structure to industrial-style Co-Mo-S catalysts remains ambiguous because the incorporation of Co into MoS_2 nanocrystals is sensitive to the synthesis procedure,[3] and because element identification at the edges of the industrial-style Co-Mo-S catalysts has so far lacked single-atom sensitivity.[8,9]

Recent advances in high-resolution (scanning) transmission electron microscopy ((S)TEM) imaging have opened up the possibility of studying two-dimensional materials with atomic-level resolution and sensitivity.[9-14] For instance, high-resolution TEM resolved the elemental distribution in single- and double-layer MoS_2 nanocrystals,[13] and high-angle annular dark-field (HAADF) STEM allowed for a distinction of the edge terminations.[14] Herein, we address the location of Co promoter atoms in the industrial-style Co-Mo-S catalysts. Figure 1a is a representative HAADF-STEM image of a hexagonally shaped Co-promoted MoS_2 nanocrystal supported on a graphite flake, oriented with its (001) basal plane along the graphite (001) plane, and orthogonal to the electron beam direction. In the HAADF mode, the images are dominated by Z-contrast, which associates a bright contrast to atomic column positions, and which, to a good approximation, scales with the square of the total projected atomic number of the columns. As in previous work,[14] the Z-contrast images of the MoS_2 basal plane present an asymmetric dumbbell structure reflecting a pair of atomic columns separated by 0.18 nm in <001> projection. This asymmetric dumbbell corresponds to 1Mo and 2S columns, indicating the presence of single-layer MoS_2 nanocrystal and facilitating the assignment of Mo- and S-edge terminations (Figure 1a).[14] Although image contrast quantification is in principle applicable to identify the type of all the atoms, in practice, the analysis usually suffers from uncertainties arising from a non-uniform support contrast and the limited signal-to-noise ratio (S/N) required for non-invasive observations with electron beams.[11,14] Therefore, to unambiguously determine the chemical arrangement of industrial-style Co-Mo-S nanocrystals, the present study combines HAADF-STEM with simultaneous electron energy-loss (EEL) spectroscopy.[15]

First, for the MoS_2 nanocrystal in Figure 1a, a spectrum image, which consists of EEL spectra recorded serially pixel-by-pixel across a selected edge region, is used to determine the elemental content from the relative intensities of the S $L_{2,3}$, Mo $M_{4,5}$ and Co $L_{2,3}$ ionization edges (Figure S1). Figures 1b-1i show the resulting elemental maps for the (100) Mo- and (-100) S-edge terminations of the MoS_2 nanocrystal. The maps reveal that the basal plane consists of Mo and S, and that S and Mo are the only constituent elements at the Mo-edge.[14] The spectrum image also contains a C *K* signal (not reported) arising from the graphite support. Here, the main finding is that the elemental maps unambiguously show a clear Co signal, which is confined to the sole S-edge, and which has an appreciable intensity at the outer atomic row. This preference for Co to occupy positions at the S-edge was confirmed in six additional single-layer MoS_2 nanocrystals (e.g. Figure S5). Interestingly, the Co maps show that the promoter atoms tend to fully cover the S-edge, even in the presence of defects (Figure S6b).

Next, the precise atomic structure and stoichiometry at the S-edge of the single-layer Co-Mo-S nanocrystal is determined by comparing the elemental maps and the HAADF-STEM image. Figure 2 shows an analysis for the S-edge in Figure 1. The 2S and 1Mo column arrangement of the basal plane lattice is readily inferred from the HAADF contrast (Figure 2a). The 2S columns coincide with maxima in the S map (Figure 2c). However, due to the inelastic scattering process[16] and low S/N, the Mo maps shown here are not atomically resolved. Nevertheless, figures 2b and 2d show that the Co signal peaks mainly at the Z-contrast maxima next to the 2S columns at the basal plane edge and that the Z-contrast maxima appear slightly fainter than the Mo columns: these maxima are therefore attributed to Co. Thus, the combination of the atomic positions indicated by Z-contrast and the element type identified by EEL spectroscopy shows unambiguously that Co atoms are occupying positions similar to Mo-sites as an extension of the MoS_2 basal plane, and that Co forms 2S-1Co dumbbells, as

[*] Y. Zhu, M. Brorson, P. G. Moses, L. P. Hansen, S. Helveg
Haldor Topsøe A/S
Nymøllevej 55, 2800 Kgs. Lyngby (Denmark)
E-mail: sth@topsoe.dk
Q. M. Ramasse
SuperSTEM Laboratory, STFC Daresbury
Keckwick Lane, Daresbury WA4 4AD (UK)
C. Kisielowski
Joint Center for Artificial Photosynthesis, National Center for Electron Microscopy, Lawrence Berkeley National Laboratory
1 Cyclotron Road, Berkeley, CA 94708 (USA)

[**] Microscopy was performed at the SuperSTEM Laboratory, Daresbury supported by the EPSRC (UK). The Danish Council for Strategic Research (grant Cat-C) and the Danish Council for Independent Research (grant HYDECAT) are gratefully acknowledged for financial support.

viewed in the MoS_2 <001> projection. Inspection of the Z-contrast line profiles also reveals that the 2S-1Co separation of ~ 0.16 nm (Co-S bond length: ~ 0.22 nm) is shorter than the 2S-1Mo separation of 0.18 nm (Mo-S bond length: 0.24 nm) (Figure S2). Further away from the edge, the EEL spectra show that Mo and Co are absent, but that S is still detected. The S signal (albeit not as well defined as in the bulk of the nanocrystal due to a lower S/N) peaks at very faint Z-contrast maxima bridging the Co atoms at the very edge of the nanocrystal (Figure 2a). These maxima have just half of the S intensity of the 2S columns on the basal plane (Figure 2e) and are correspondingly assigned to single S atoms. Z-contrast line profiles show that the 1Co-1S separation is 0.19-0.22 nm, again consistent with a contraction of the Co-S bond length compared to that of Mo-S. Thus, the 2S-1Co dumbbells at the S-edge are terminated by a row of single S atoms such that the Co atoms are tetrahedrally coordinated to S.

As a note of caution, the acquisition of the present data at single-atom sensitivity requires low electron doses because the catalyst is highly susceptible to electron beam damage. Such effects appear as atom removal (mainly at edges or corners) between successive images (Figure S6 and S7). To address the impact of the electron beam, HAADF-STEM images were therefore recorded before and after the spectroscopic data acquisition. Only spectroscopic results without noticeable lattice damage in those images were included in the present analysis (Figures S5-S7).

Figure 3 summarizes the analysis in an atomistic picture: the industrial-style carbon-supported Co-Mo-S nanocrystals have single Co atoms preferentially located at the S-edge of a MoS_2 nanocrystal and coordinated tetrahedrally to S atoms. The structure of the unpromoted Mo-edge termination of the MoS_2 nanocrystal was addressed previously (Figure S3).[14] The preferred location of Co in the present industrial-style Co-Mo-S nanocrystals agrees with previous STM[5,6] and DFT[6,7] studies. These studies considered Co-Mo-S nanocrystals formed on Au(111) by a physical vapor deposition method under ultra-high vacuum conditions, or in an unsupported state, respectively. Moreover, the observed contracted Co-S bond length and the tetrahedral S coordination of Co agrees with X-ray absorption spectroscopy results from industrial-style alumina- and carbon-supported Co-Mo-S catalysts.[17] The comparison of the different model and industrial-style Co-Mo-S catalysts shows similar structural characteristics, despite remarkable differences in their preparation, support and sulfidation. In fact, the observations of the 1S reconstruction at the Co-promoted S-edge and at the unpromoted Mo-edge agree with DFT calculations of unsupported Co-Mo-S.[7b,14,18] This correspondence indicates that the present sulfiding conditions are adequate to equilibrate edge structures and that the Co-Mo-S/graphite interaction is sufficiently weak to leave that equilibrium structure unperturbed.

However, a part of the MoS_2 nanocrystals inspected in the Co-promoted catalyst deviated from the Co-Mo-S structure. Figure 4a shows a single-layer MoS_2 nanocrystal for which the EEL spectra unambiguously reveal a Co $L_{2,3}$ edge as well as an additional Fe $L_{2,3}$ edge (Figure 4b-d). The atom-by-atom analysis shows that Co and Fe atoms occupy similar sites (Figure 4c). This similarity agrees with previous model studies[19] and may arise because Co and Fe are neighboring transition metals, as opposed to W or Au that substitute into basal plane sites or lattice defects[4,20], respectively. However, Fe was not intentionally added during the present synthesis. Therefore, the observed Fe (Figure 4b) probably stems from the Fe residuals detected in the graphite support (Experimental Section).

In summary, the present analysis of an industrial-style, carbon-supported Co-Mo-S catalyst reveals that single Co promoter atoms are located preferentially at the S-edges with a tetrahedral coordination to S. As a result, the Co-promoter atoms become intrinsically undercoordinated to S, an arrangement which has previously been proposed to be attractive for adsorption of S-containing reactants.[5,6,7b] Moreover, the direct characterization of the Co-Mo-S structure agrees well with complementary studies of model and industrial-style catalysts. This independence of the synthesis route and support material suggests that the Co-Mo-S structure represents an equilibrated phase. The observations therefore give hope that further interplay with model studies will uncover the role of the Co- promoter in the industrial HDS catalysis. However, the fact that Fe residuals compete with Co for S-edge sites suggests that the Co-Mo-S preparation is highly sensitive to the purity of the raw materials. As Fe does not to promote the HDS activity,[3,20] its presence lowers the fraction of the promoted Co-Mo-S sites. This finding may explain why carbon-supported Co-Mo-S catalysts tend to vary in activity depending on the type of carbon.[3] Thus, the present analytical capability of pinpointing local atomic stoichiometry should in general be highly beneficial for developing preparative routes of promoted MoS_2 catalysts and other nanomaterials with tunable functionalities.

Experimental Section

The industrial-style Co-promoted MoS_2 hydrotreating catalyst was prepared on a graphitic support by a sequential incipient wetness impregnation method.[21] First, a graphitic powder (Grade AO-2, Graphene Supermarket) was rinsed by oxalic acid to reduce metallic impurities, resulting in a residual Fe content of about 210 ppm. Secondly, the rinsed powder was tabletized and granulated. The graphite granulates were (i) impregnated by a Co (acetate) solution of 0.1 wt% Co, (ii) dried in ambient at 110 ℃, (iii) dipped in an $(NH_4)_2[MoS_4]$ solution with a Mo loading of around 0.3 wt% and (iv) finally dried. Thus, the nominal atomic ratio of Mo:Co was 3:1. Finally, the impregnated graphite was sulfided in 10% H_2S in H_2 at 1073 K for 6 hours and subsequently cooled to room temperature in inert N_2. The samples were stored in a dry and O_2-free atmosphere, which is also used for TEM sample preparation.[13,14] Specifically, granulates were crushed in a mortar and dispersed dry on standard Cu TEM-grids covered with lacey carbon.

Electron microscopy was carried out at the SuperSTEM Laboratory, Daresbury, using a Nion UltraSTEM100 dedicated aberration-corrected scanning transmission electron microscope. The microscope has an ultra-high vacuum below 5×10^{-9} Torr near the sample. The instrument is equipped with a cold field emission gun with a native energy spread of 0.35 eV and was operated with a beam energy of 60 keV. The probe-forming optics was configured to provide a beam convergence semi-angle of 30 mrad, corresponding to a probe size of ca. 0.11 nm. An estimated electron beam current of ca. 50 pA was impinging on the sample. STEM images were acquired in HAADF mode with the detector inner and outer radii being calibrated at 85 mrad and 190 mrad, respectively. EEL spectrum images were recorded using a Gatan Enfina spectrometer, with a collection semi-angle of 37 mrad. An energy dispersion of 0.7 eV/channel was chosen so the S $L_{2,3}$, Mo $M_{4,5}$ and Co $L_{2,3}$ ionization edges could all be recorded simultaneously. The dwell time was set to 50 ms/spectrum, which provided the best achievable compromise between acquisition speed and S/N.[22] The data in Figure 1, 2 and 4 are simultaneously recorded HAADF-STEM and EEL spectrum images. In the analysis, all spectrum images were first denoised using principal component analysis.[23] Subsequently, the electron energy dispersion was carefully calibrated using the S $L_{2,3}$ and Fe $L_{2,3}$ ionization edge onsets as internal references, while the C K edge onset was used to check for energy shifts. For generating elemental maps, the spectra were background-subtracted by fitting a power law model to electron energies lower than the edge onsets, without any further smoothing or filtering, and integrated over a 20 eV, 40 eV and 60 eV windows above the edge onset of the S $L_{2,3}$, Mo $M_{4,5}$ and Co $L_{2,3}$ signals at each spatial pixel (unless specified otherwise). HAADF-STEM images are reported as raw data, unless otherwise specified.

Keywords: electron energy loss spectroscopy • electron microscopy • heterogeneous catalysis • molybdenum disulfide • single-atom sensitivity

[1] a) R. Tenne, *Angew. Chem.* **2003**, *115*, 5280-5289; Angew. Chem. Int. Ed. **2003**, *42*, 5124-5132; b) Q. H. Wang, K. Kalantar-Zadeh, A. Kis, J. N. Coleman, M. S. Strano, *Nature Nanotechnology* **2012**, *7*, 699-712; c) M. Chhowalla, H. S. Shin, G. Eda, L. J. Li, K. P. Loh, H. Zhang, *Nature Chem.* **2013**, *5*, 263-275.

[2] a) F. Besenbacher, M. Brorson, B. S. Clausen, S. Helveg, B. Hinnemann, J. Kibsgaard, J. V. Lauritsen, P. G. Moses, J. K. Nørskov, H. Topsøe, *Catal. Today* **2008**, *130*, 86-96; b) T.F. Jaramillo, K.P. Jørgensen, J. Bonde, J.H. Nielsen, S. Horch, I. Chorkendorff, *Science* **2007**, *317*, 100-102.

[3] H. Topsøe, B. S. Clausen, F. E. Massoth, *Hydrotreating Catalysis*, Springer, **1996**.

[4] Y. F. Chen, J. Y. Xi, D. O. Dumcenco, Z. Liu, K. Suenaga, D. Wang, Z. G. Shuai, Y. S. Huang, L. M. Xie, *ACS Nano* **2013**, *7*, 4610-4616.

[5] J. V. Lauritsen, S. Helveg, E. Lægsgaard, I. Stensgaard, B. S. Clausen, H. Topsøe, F. Besenbacher, *J. Catal.* **2001**, *197*, 1-5.

[6] J. V. Lauritsen *et al* , *J. Catal.* **2007**, *249*, 220-233.

[7] a) L. S. Byskov, J. K. Nørskov, B. S. Clausen, H. Topsøe, *J. Catal.* **1999**, *187*, 109-122; b) H. Schweiger, P. Raybaud, H. Toulhoat, *J. Catal.* **2002**, *212*, 33-38.

[8] O. Sørensen, B. S. Clausen, R. Candia, H. Topsøe, *Appl.Catal.* **1985**, *13*, 363-372.

[9] F. L. Deepak, R. Esparza, B. Borges, X. Lopez-Lozano, M. Jose-Yacaman, *ACS Catal.* **2011**, *1*, 537-543.

[10] C. O. Girit *et al*, *Science* **2009**, *323*, 1705-1708.

[11] O. L. Krivanek *et al*, *Nature* **2010**, *464*, 571-574.

[12] K. Suenaga, M. Koshino, *Nature* **2010**, *468*, 1088-1090.

[13] C. Kisielowski, Q. M. Ramasse, L. P. Hansen, M. Brorson, A. Carlsson, A. M. Molenbroek, H. Topsøe, S. Helveg, *Angew. Chem.* **2010**, *122*, 2768-2770; *Angew. Chem. Int. Ed.* **2010**, *49*, 2708-2710.

[14] L. P. Hansen, Q. M. Ramasse, C. Kisielowski, M. Brorson, E. Johnson, H. Topsøe, S. Helveg, *Angew. Chem.* **2011**,*123*, 10172-10175; *Angew. Chem. Int. Ed.* **2011**, *50*, 10153-10156.

[15] P. E. Batson, *Nature* **1993**, *366*, 727-728.

[16] L. J. Allen, S. D. Findlay, M. P. Oxley, in *Scanning Transmission Electron Microscopy* (Eds.: S. J. Pennycook, P. D. Nellist), Springer, **2011**, pp. 247-290.

[17] a) B. S. Clausen, B. Lengeler, R. Candia, J. Als-Nielsen, H. Topsøe, *Bull. Soc. Chim. Belg.* **1981**, *90*, 1249-1259. b) S.M M. A. M. Bouwens, J. A. R. van Veen, D. C. Koningsberger, V. H. J. de Beer, R. Prins, *J. Phys. Chem.* **1991**, *95*, 123.

[18] P. G. Moses, B. Hinnemann, H. Topsøe, J. K. Nørskov, *J. Catal.* **2009**, *268*, 201-208.

[19] J. Kibsgaard, A. Tuxen, K. G. Knudsen, M. Brorson, H. Topsøe, E. Lægsgaard, J. V. Lauritsen, F. Besenbacher, *J. Catal.* **2010**, *272*, 195-203.

[20] Y.C. Lin, D. O. Dumcenco, H.-P. Komsa, Y. Niimi, A. V. Krasheninnikov, Y.-S. Huang, K. Suenaga, *Adv. Mater.* **2014**, *26*, 2857-2861.

[21] M. Brorson, A. Carlsson, H. Topsøe, *Catal. Today* **2007**, *123*, 31-36.

[22] R. Zan, Q. M. Ramasse, R. Jalil, T. Georgiou, U. Bangert, K. S. Novoselov, *ACS Nano* **2013**, *7*, 10167–10174.

[23] N. Bonnet, N. Brun, C. Colliex, *Ultramicroscopy* **1999**, *77*, 97-112.

Figure 1. a) Unprocessed HAADF-STEM image of a single-layer Co-Mo-S nanocrystal on a graphite support with MoS_2 (001) orthogonal to the electron beam direction (left). A ball model and an enlarged section of the interior lattice (right), showing the asymmetric 2S-1Mo dumbbell Z-contrast pattern, resolves the (100) Mo- and (-100) S-edge terminations as marked. Simultaneously recorded HAADF-STEM image and elemental maps are derived from the S $L_{2,3}$, Mo $M_{4,5}$ and Co $L_{2,3}$ ionization edges at the Mo-edge (b-e) and S-edge (f-i). Note that the S maps are atomically-resolved with maxima at the S sublattice of the basal plane while the Mo maps only provides a reference for the distribution of Mo. Arrows mark the termination of the basal MoS_2 (open) and the position of Co (red). The Co map also shows faint maxima suggesting near-atomic resolution.

Figure 2. a) High-resolution HAADF-STEM image of the S-edge in Figure 1a and corresponding (b) Mo and Co and (c) S maps. The ball model denotes the positions of a 1Mo (blue), 2S (yellow), 1Co (red) and 1S (orange) atom columns (Figure S2). d) Integrated Co $L_{2,3}$ ionization edge, representing the sum from six different 1Co atomic columns along the S edge. e) The $L_{2,3}$ edges of one 2S and one 1S atomic column in c). Each atomic-column EEL spectrum is integrated over a window of 3 x 3 pixel area (corresponding to the probe size) in a).

Figure 3. Top-view ball model of the industrial-style Co-Mo-S nanocrystal. The balls denote the position of 1Mo (blue), 1Co (red), 2S (yellow) and 1S (orange) column.

Figure 4. a) HAADF-STEM image of a MoS_2 nanocrystal. An EEL spectrum image is acquired over the S-edge area framed in black. b) The corresponding combined Mo+Co+Fe map. Here, the Fe and Co signals are integrated over a 40 eV window above their respective edge onsets. c) HAADF image at the S-edge (framed in a) with a superimposed ball model indicating 1Co (red), 1Fe (green), 1Mo (blue), 2S (yellow) and 1S (orange) column positions. d) Separate EEL spectra integrated over the white-framed regions in b showing Fe and Co $L_{2,3}$ ionization edges. A slight structural change of (a removed Co atom, marked by an open circle) does not affect the conclusion (Figure S4c).

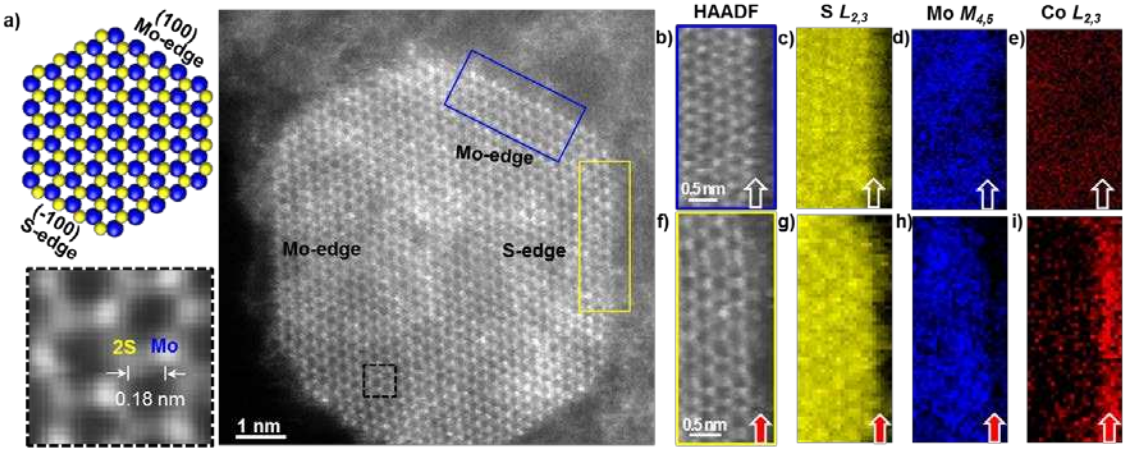

Figure 1

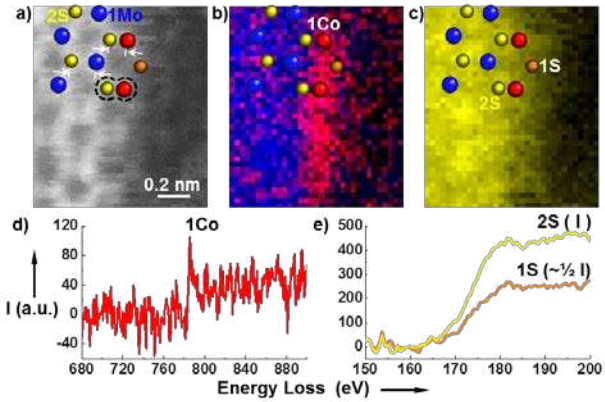

Figure 2

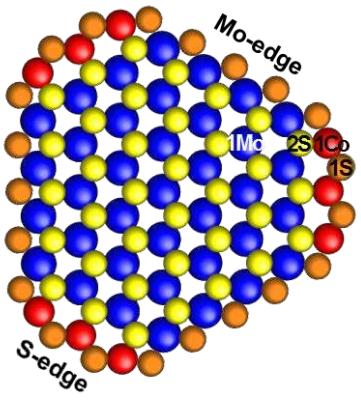

Figure 3

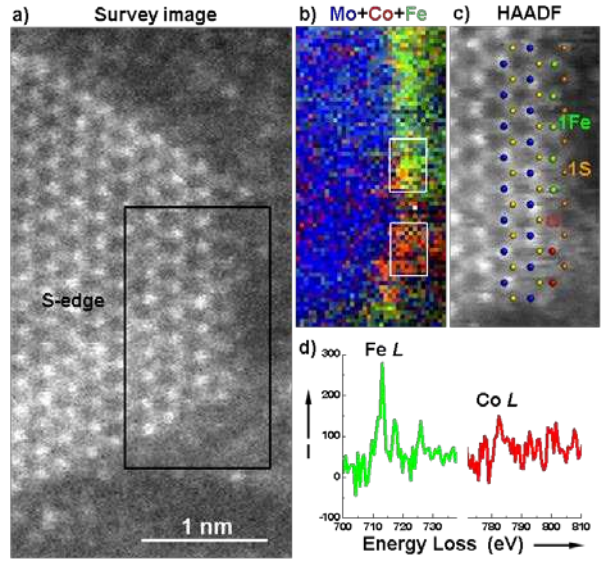

Figure 4